Article submitted to: High Power Laser Science and Engineering, 2023 *July 20, 2023*

All-optical non-linear chiral ultrafast magnetization dynamics driven by circularly polarized magnetic fields

Luis Sánchez-Tejerina[1,2], Rodrigo Martín-Hernández[1], Rocío Yanes[3], Luis Plaja[1], Luis López-Díaz[3], and Carlos Hernández-García[1]

[1]*Grupo de Investigación en Aplicaciones del Láser y Fotónica, Departamento de Física Aplicada, Universidad de Salamanca, E-37008, Salamanca, Spain.*
[2]*Present address: Departamento de Electricidad y Electrónica, Universidad de Valladolid, 47011 Valladolid, Spain*
[3]*Departamento de Física Aplicada, Universidad de Salamanca, E-37008, Salamanca, Spain*

Abstract
Ultrafast laser pulses provide unique tools to manipulate magnetization dynamics at femtosecond timescales, where the interaction of the electric field usually dominates over the magnetic field. Recent proposals using structured laser beams have demonstrated the possibility to produce regions where intense oscillating magnetic fields are isolated from the electric field. In these conditions, we show that technologically feasible Tesla-scale circularly polarized high-frequency magnetic fields induce purely precessional nonlinear magnetization dynamics. This fundamental result not only opens an avenue in the study of laser-induced ultrafast magnetization dynamics, but also sustains technological implications as a route to promote all-optical non-thermal magnetization dynamics both at shorter timescales—towards the sub-femtosecond regime— and at THz frequencies.

Keywords: Ultrafast dynamics, Non-linear dynamics, Chiral behavior

1. Introduction

The pioneering work on ultrafast demagnetization in Ni[1] paved the way towards a large number of theoretical and experimental studies on magnetization dynamics at the femtosecond (fs) time scales induced by ultrashort laser pulses[2–25]. In these studies the dynamics is mediated primarily by the electric field (E-field), which can excite non-equilibrium states[5–9], demagnetize the sample,[1,14–21] generate localized charge currents[24,25], or induce the inverse Faraday effect[22,23]. While most of the techniques are mediated mainly by the E-field, other techniques, such as the excitation of phononic modes[26], have recently provided routes for non-thermal magnetization manipulation.

An appealing alternative to induce coherent magnetization dynamics consists on the use of magnetic fields (B-field). The role of the B-field in ultrafast magnetization dynamics has been extensively studied, specially in the regime of linear response to THz fields[27–32]. At this picosecond time scale, few Tesla (T) are required to introduce small deflections from the equilibrium magnetization direction, while tens of T are needed for achieving complete switching. Higher driving frequencies, that could break into the femtosecond timescale, would require very high B-field amplitudes. Although intense magnetic fields can be achieved, for example, using plasmonic antennas[33], in such regime, the associated E-field would potentially demagnetize the sample[34] or even damage it. Besides, although substantial advances have been made towards the generation of electromagnetic fields in the range of THz (0.1 to 30 THz), their intensity is still small as compared to the infrared case[35–37].

In this work we introduce an appealing alternative to drive magnetization dynamics at the sub-picosecond timescale, by using isolated ultrafast intense B-fields. Recent developments in structured laser sources have demonstrated the possibility to spatially decouple the B-field from the E-field of an ultrafast laser pulse. For instance, azimuthally-polarized laser beams present a longitudinal B-field at the beam axis, where the E-field is zero[38]. Depending on the laser beam parameters, the contrast between the longitudinal B-field and the radial B-field and the E-field can be adjusted, so to design a local region in which the longitudinal B-field can be considered to be isolated from both, radial B-field and E-field[39]. In such region, the stochastic processes driven by the E-field could be avoided, and the coherent

Correspondence to: Email: luis.sanchez-tejerina@uva.es

10.1017/hpl.2023.71
https://doi.org/10.1017/hpl.2023.71 Published online by Cambridge University Press

precession induced by the B-field can be exploited.Besides, only the longitudinal component of the B-field is present and, consequently, the magnetic field is linearly polarized. Indeed, azimuthally-polarized laser beams have been shown to induce isolated mili-Tesla static B-fields[40], with applications in nanoscale magnetic excitations and photoinduced force microscopy[41,42]. More recently, ultrafast time-resolved magnetic circular dichroism has been proposed[43]. In addition, theoretical proposals[39,44] and experiments[45,46] have raised the possibility to generate isolated Tesla-scale fs magnetic fields by the induction of large oscillating currents through azimuthally polarized fs laser beams.

Our theoretical study unveils the non-linear, chiral, precessional magnetization response of a standard ferromagnet to a Tesla scale circularly polarized ultrafast magnetic field whose polarization plane contains the initial equilibrium magnetization. First, we show in section 2 the feasibility to use state-of-the-art structured laser beams to create a macroscopic region in which such B-fields are found to be isolated from the E-field by particle-in-cell (PIC) simulations. It is worth to mention that this circularly polarized B-field is a non-propagating solution which shall not be confused with a circularly polarized structured laser beams as those considered in[47]. Then, we present our micromagnetic (μMag) simulations for moderate fields in section 3 showing the presence of measurable magnetization dynamics in CoFeB when a circularly polarized 10 ps B-field pulse of 10 T and central frequency 30 THz is applied. Additionally, we compare the dynamics triggered by a B-field with linear polarization, circular polarization with the polarization plane perpendicular to the equilibrium magnetization, and circular polarization with the polarization plane parallel to the equilibrium magnetization. Measurable magnetization dynamics are found in the later case. In section 4, we provide for a complete analytical model to describe such dynamics, and compare it with full μMag simulations. This model allows us to predict the complete magnetization switching by using 1 ps, 275 T, 60 THz, B-field pulses, verifed by full μMag simulations. Finally, section 5 summarizes the main conclusions of the work and gives some perspectives on possible implications in the field.

2. Spatially isolated circularly polarized B-fields out of structured laser beams

In order to study the interaction of an isolated, circularly polarized B-field with a standard ferromagnet (CoFeB), we consider a B-field, **B**, oscillating in the xz plane (see Fig. 1(a)) given by

$$\mathbf{B}(t) = \mathbf{b}(t)\, e^{i\omega t} + \mathbf{b}^{*}(t)\, e^{-i\omega t} \tag{1}$$

$$\mathbf{b}(t) = \frac{B_0}{2} F(t) \left(\cos\theta_0 \hat{u}_x + \sin\theta_0 e^{i\phi_0} \hat{u}_z\right), \tag{2}$$

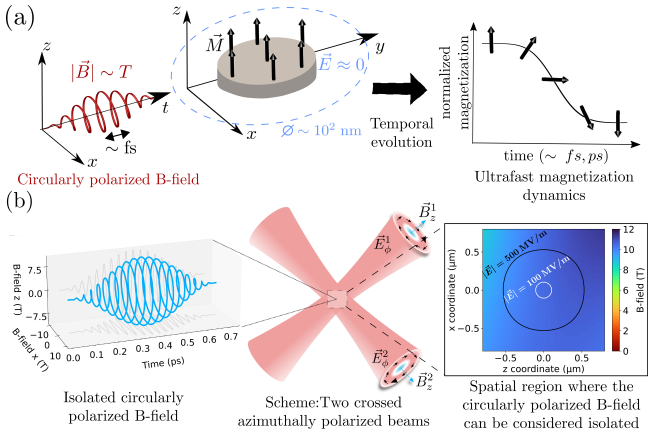

Figure 1. a) Sketch of the system under consideration. A circularly polarized magnetic field illuminates a magnetic sample whose dimensions are smaller than the region for which the E-field can be considered negligible. This field can trigger ultrafast magnetization dynamics. b) Two crossed azimuthally polarized beams of 30 THz and peak intensity 2.1×10^{13} W/cm^2 define a spatial region of $\simeq$ 100 nm in which the E-field is lower than 100 MV/m, as depicted in panel. In such region, a constant circularly B-field of amplitude 10.5 T and central frequency 30 THz is found.

where ω is the central angular frequency, ($\omega = 2\pi f$), B_0 is the amplitude, and θ_0 and ϕ_0 define the relative amplitude and phase between the x and z components, respectively. $F(t)$ is the field envelope, given by $F(t) = \sin^2(\pi t/T_p)$ for $0 \leq t \leq T_p$, with $T_p = 3/8 t_p$ its full duration, t_p being the full-width-at-half-maximum (FWHM) pulse duration in intensity. A right-handed—RCP— (left-handed—LCP—) circularly polarized B-field in the xz plane corresponds to $\phi_0 = \pi/2$ ($\phi_0 = -\pi/2$) and $\theta_0 = \pi/4$, while a linearly polarized B-field corresponds to $\phi_0 = 0$ or π.

In our simulations, we do not include any E-field coupling, as the B-field is assumed to be isolated. Such assumption is valid for CoFeB in spatial regions where the E-field is lower than 100 MV/m, for which the demagnetization has been predicted to be less than 7%[14,48]. The conditions for which an intense circularly polarized B-field can be found spatially isolated from the E-field can be obtained by using two crossed azimuthally polarized laser beams, as sketched in Fig. 1(b). We have performed PIC simulations using the OSIRIS 3D PIC code[49–51], in order to show how such isolated B-fields can be achieved with the state-of-the-art ultrafast laser technology. We have considered two orthogonal azimuthally polarized laser beams with waist $w_0 = 3.125\lambda = 31.25$ μm, a central wavelength of $\lambda = 10$ μm (30 THz), and E-field amplitude of 12.5 GV/m (peak intensity of 2.1×10^{13} W/cm^2) at their radius of maximum intensity, $w_0/\sqrt{2}$. The temporal envelope is modeled as a sin^2 function of 88.8 fs FWHM. Due to computational limitations the temporal envelope is much shorter than those considered in the μMag simulations presented in this work, which lies in the ps regime. However, we do not foresee any deviation in the results presented if longer pulses with similar amplitudes are considered.

https://doi.org/10.1017/hpl.2023.71 Published online by Cambridge University Press

In Fig. 1(b) we also show the spatial distribution of the B-field (color background) and the E-field (contour lines) at overlapping region. We have highlighted the region in which the E-field is lower than 100 $\mathrm{MV/m}$, and thus the E-field can be neglected against the B-field. Thus, we can define a region of radius $\simeq$ 100 nm in which the B-field exhibits a constant amplitude of 10.5 T and the E-field is maintained below 100 MV/m. Though the use of additional currents, like in Refs.[39,44], could enhance the B-field amplitude, our simulations demonstrate that moderately intense laser beams can already reach the B-field amplitudes required to observe the non-linear magnetization dynamics described below.

3. Nonlinear magnetization response to ultrafast B-fields

The interaction between the oscillating B-field and the magnetization is given by the Landau-Lifshitz-Gilbert (LLG) equation[29,52]

$$\left(1+\alpha^2\right)\frac{d\mathbf{m}}{dt} = -\gamma\mathbf{m}\times\mathbf{B}_{eff} - \alpha\mathbf{m}\times(\mathbf{m}\times\mathbf{B}_{eff}) \quad (3)$$

where **m** is the normalized magnetization where both spatial and temporal dependencies are implicitly assumed, α is the Gilbert damping parameter, and $\mathbf{B}_{eff}$ is the effective magnetic field. We have performed μMag simulations using the well-known software MuMax^3[53] to solve the LLG equation. The system under study is sketched in Fig. 1(a), where we consider a circular nanodot with 1 nm thickness and 64 nm diameter discretized into 1 nm cubic cells. The material parameters correspond to CoFeB grown over a heavy metal layer: inhomogeneous exchange parameter $A = 19$ pJ/m, saturation magnetization $M_S = 1$ MA/m, perpendicular uniaxial anisotropy (i.e. the anisotropy field is directed along the z direction) parameter $K_u = 800$ kJ/m^3, Dzyaloshinkii-Moriya interaction (DMI) $D = 1.8$ mJ/m^2 and Gilbert damping $\alpha = 0.015$.

In Fig. 2(a) we show the in-plane magnetization dynamics (perpendicular to the equilibrium configuration, $m_z = 1$) induced by RCP and LCP B-fields lying in the xz plane. Note that the equilibrium magnetization lies in the polarization plane. In both cases, $B_0 = 10$ T, $f = 30$ THz, and $t_p = 10$ ps. We can observe a magnetization precession around the z axis triggered by a non-linear chiral response to the B-field. While the RCP B-field induces a measurable negative x component, the LCP leads to a positive one. After the pulse, the precession dynamics is dominated by the anisotropy field, and the system starts to precess around the z-axis. Note that the broad trace is due to the subsequent magnetization oscillations during the interaction with the pulse.

The non-linear mechanism underlying such behavior can be understood as follows (see bottom part of Fig. 2(a)). At an initial time $t = 0$, in which **m** (black arrow) lies in the polarization plane of the circularly polarized B-field

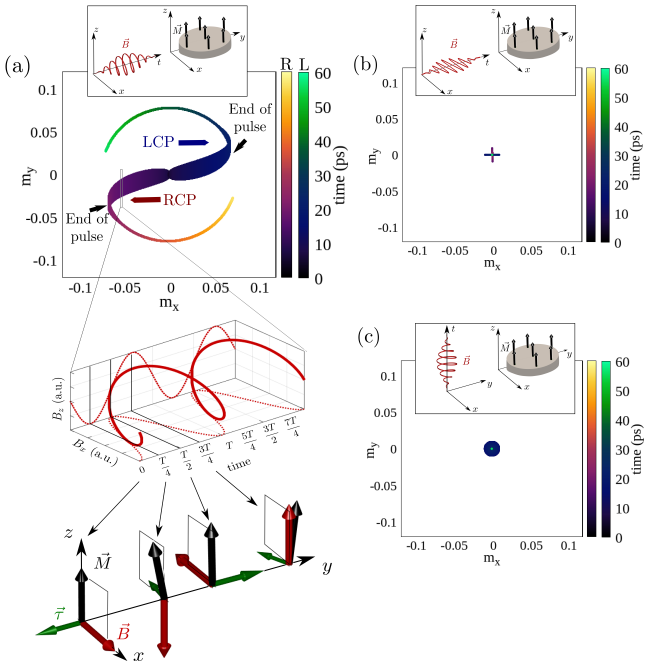

Figure 2. Micromagnetic simulation results of the temporal evolution (color code) of the magnetization components (m_x, m_y) of CoFeB excited by B-fields with different polarization states. a) RCP (yellowish color scale) and LCP (greenish color scale) B-fields ($B_0 = 10$ T, $f = 30$ THz, $t_p = 10$ ps). The RCP (LCP) B-field induces a measurable negative (positive) m_x component. In both cases the anisotropy field induces a precession of **m** around the equilibrium configuration. The bottom part sketches the mechanism during a B-field period of constant amplitude. The B-field (red), magnetization (black) and torque (green) vector representations at four different times reveal the magnetization dynamics mechanism over one period. b) Linear polarization along x (yellowish trace) or y (greenish trace). c) Circular polarization perpendicular to the equilibrium magnetization with RCP (yellowish trace) and LCP (greenish trace) helicities.

(red arrow), being perpendicular to it, a transverse torque τ (green arrow) drives **m** out-of-plane from this initial position. During the next quarter-period, τ decreases and rotates, inducing a precession of **m** around its initial axis. For the second quarter-period, τ increases again keeping its rotation but, at $t = T/2$, it reverses its rotation direction, thus sweeping only half of the plane perpendicular to **m**. As a result, along a whole period, the torque component perpendicular to the polarization plane averages to zero, while a residual contribution along the intersection of the polarization plane and the plane perpendicular to **m** remains. With long lasting multicycle laser pulses it is then possible to accumulate the small torque along the polar coordinate on the polarization plane, θ, so as to promote the system to a targeted non-equilibrium state. This is reflected in Fig. 2(a), where the magnetization components m_x and m_y are non-zero at the end of the pulse, and therefore the magnetization is not aligned along the anisotropy direction, z. A more detailed scheme of the non-linear mechanism is displayed in Supplementary Videos 1 and 2 for both, RCP and LCP B-fields, revealing the chiral nature of the reported effect.

To highlight the importance of the polarization state and

https://doi.org/10.1017/hpl.2023.71 Published online by Cambridge University Press

orientation to get the non-linear response, Figs. 2(b) and 2(c) depict the temporal evolution of the magnetization components (m_x, m_y) obtained from full micromagnetic simulations for a linearly polarized B-field, being perpendicular to the equilibrium magnetization, and for a circularly polarized B-field (either RCP or LCP), where the polarization plane is perpendicular to the equilibrium magnetization. Whereas in both cases a small magnetization deflection is observed, the net torque exerted by the field on the magnetization over a period is null, and the magnetization recovers its equilibrium state after the B-field pulse. In addition, at frequencies larger than few tens of THz the response is not enough to promote significant change on the magnetization even for a B-field as high as $B = 10$ T. Consequently, in the cases presented in Figs. 2(b) and 2(c), the response is completely linear and the magnetization comes back to the initial configuration at the end of the B-field pulse. Nonetheless, for a circularly polarized B-field (either RCP or LCP) with the equilibrium magnetization lying in the polarization plane, the non-linear chiral phenomenon described above triggers the magnetization out of equilibrium as shown Fig. 2(a). This dragging, being a non-linear effect, is sensitive to the B-field envelope and does not cancel out at the end of the pulse.

4. Analytical model

To give insight into the nonlinear mechanism introduced in previous section and sketched in Fig. 2(a), we derive an approximated analytical model. The exchange field is not included in the model because we assume that the sample remains uniformly magnetized. Besides, we neglect the anisotropy and DMI fields—which are small if compared to the external one— and the damping term. Similar assumptions has been proven reasonable at this time scale in previous studies[29]. With these approximations in Eq. (3), the magnetization dynamics out of the polarization plane reads as

$$\frac{dm_y}{dt}\mathbf{u}_y = -\gamma' \mathbf{m}_{\parallel} \times \mathbf{B}, \tag{4}$$

$\mathbf{m}_{\parallel}$ being the magnetization in the polarization plane and $\gamma' = \gamma/\left(1+\alpha^2\right)$. Considering the initial magnetization in the z direction, m_y at any time t is given by

$$m_y(t)\,\mathbf{u}_y = -\gamma' \int_0^t \mathbf{m}_{\parallel}(\tau) \times \mathbf{B}\, d\tau. \tag{5}$$

The cartesian components of the magnetization can be decomposed at each point in its Fourier components,

$$m_j(t) = \sum_q m_q^j(t)\, e^{iq\omega t} \qquad j = \{x, y, z\}. \tag{6}$$

Using Eqs. (5) and (6) in the simplified LLG equation, we obtain

$$\sum_q \left(\frac{d\mathbf{m}_q^{\parallel}(t)}{dt} + iq\omega \mathbf{m}_q^{\parallel}(t) \right) e^{iq\omega t} = \\ +\gamma'^2 \left[\sum_q \int_0^t \mathbf{m}_{q-1}^{\parallel}(\tau) \times \mathbf{b}(\tau)\, e^{iq\omega\tau} d\tau \right] \times \mathbf{B}(t) + \\ +\gamma'^2 \left[\sum_q \int_0^t \mathbf{m}_{q+1}^{\parallel}(\tau) \times \mathbf{b}^*(\tau)\, e^{iq\omega\tau} d\tau \right] \times \mathbf{B}(t). \tag{7}$$

Assuming that the magnetization components in the polarization plane, $\mathbf{m}_{q\pm1}^{\parallel}$, and the B-field envelope, $\mathbf{b}(\mathbf{t})$, evolve slowly, considering $\mathbf{b}(0) = 0$, and selecting only the slowly varying terms ($q = 0$), Eq. (7) transforms into

$$\frac{d\mathbf{m}_0^{\parallel}(t)}{dt} = -\frac{2i\gamma'^2}{\omega} \mathbf{m}_0^{\parallel}(t) \times \left(\mathbf{b}(t) \times \mathbf{b}^*(t) \right). \tag{8}$$

It is well known that the effective field dependence on the magnetization can lead to non-linear effects[48,54,55]. However, it must be noticed that, differently from those cases, the described effect is non-linear on the external field, not on the effective field. Moreover, it is proportional to the gyromagnetic ratio and the inverse of the frequency, being equivalent to a drift magnetic field $\vec{B}_d$ given by,

$$\mathbf{B}_d = \frac{\gamma'}{2\omega} \sin\phi_0 \left(\mathbf{B}_x \times \mathbf{B}_z \right). \tag{9}$$

Using this definition, Eq. (8) describes the slowly varying LLG dynamics in terms of the drift field, $\mathbf{B}_d$. Eqs. (8) and (9) constitute the main contribution of the present work, as they reveal a second-order dependency of the magnetization dynamics with the external B-field. From Eq. (9) we can already infer that $\mathbf{B}_d$ is maximal for circular polarization, decreases with the ellipticity, and is zero for a linearly polarized B-field ($\phi_0 = 0$ or π). Note also the chiral nature of the presented mechanism, as the direction of $\mathbf{B}_d$ is helicity dependent. Finally, we stress the purely precessional nature of $\mathbf{B}_d$—being linear with the gyromagnetic ratio—and its inverse proportionality with the driving frequency. It is worth noting that a small misalignment of the azimuthally polarized laser beams would convert the circularly polarized magnetic field into elliptically polarized magnetic field, and/or would introduce a small angle between the initial magnetization and the polarization plane. Nonetheless, it is possible to decompose the total magnetic field in a circularly polarized magnetic field in the xz plane and a linearly polarized magnetic field in the y direction. However, this later component would not affect the slow dynamics presented here.

We now analyze the dependency of the magnetization dynamics on the B-field, both with the analytical model represented by Eq. (8), and the full micromagnetic simulations, where all the interactions on the effective field, as well as the damping, are included. To highlight the accuracy of our

https://doi.org/10.1017/hpl.2023.71 Published online by Cambridge University Press

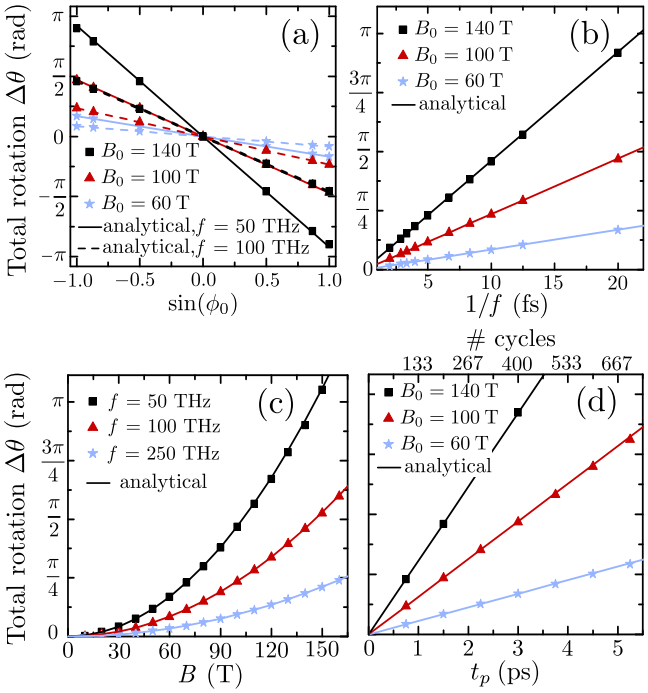

Figure 3. Analysis of the nonlinear effect dependencies Total magnetization rotation as a function of **(A)** the polarization state of the B-field (characterized by ϕ_0, and using $\theta_0 = \pi/4$), and **(B)** the inverse of the frequency of a circularly polarized B-field. In both, **(A)** and **(B)** three different B-field amplitudes (60 T blue, 100 T red and 140 T black) oscillating at $f = 50$ THz are represented. **(C)** Total magnetization rotation as a function of the circularly polarized B-field amplitude, with three different central frequencies ($f = 50$ THz blue, $f = 100$ THz red and $f = 250$ THz black). In **(A)**, **(B)** and **(C)** the B-field pulse duration is $t_p = 3$ ps. **(D)** Total magnetization rotation as a function of the circularly polarized B-field pulse duration, t_p, with three different B-field amplitudes (60 T blue, 100 T red and 140 T black) and a central frequency of $f = 50$ THz. In all panels symbols indicate results from micromagnetic simulations while lines correspond to Eq. (10).

model based on the equivalent drift field, we compare the total rotation of the magnetization from our simulations with the magnetization rotation induced by the drift B-field, $\mathbf{B}_d$, which can be computed as

$$\Delta\theta = \gamma' \left[\frac{\gamma'}{2\omega} \sin\phi_0 \left(B_x B_z\right) \right] t_p. \qquad (10)$$

Fig. 3, presents the induced magnetization rotation as derived from the analytical model (solid lines) and the micromagnetic simulations (dots). The excellent agreement allows us to validate our model and demonstrate the reported non-linear chiral effect. First, Fig. 3(a) shows the total rotation of the magnetization as a function of the polarization state (characterized by ϕ_0) of an external B-field of $t_p = 3$ ps, for amplitudes of 60 T (blue) , 100 T (red) and 140 T (black). Our simulations confirm no rotation for a linearly polarized B-field, and a maximum rotation for circular polarization. The chiral character of the phenomenon is also evidenced.

Fig. 3(b) depicts the inverse dependency of the magnetization rotation with the B-field frequency. This frequency

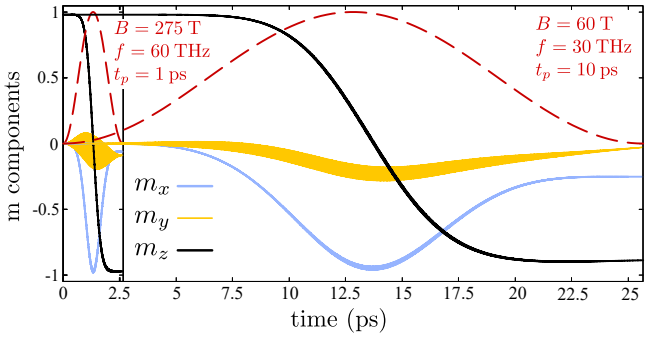

Figure 4. Micromagnetic simulation results of the temporal evolution of the magnetization components (m_x blue, m_y yellow, m_z black) of CoFeB excited by a RCP B-field. The normalized B-field envelope is shown in dashed-red. While a B-field of $B_0 = 60$ T, $f = 30$ THz, and $t_p = 10$ ps shows switching at the ps timescale, a B-field of $B_0 = 275$ T, $f = 60$ THz, and $t_p = 1$ ps achieves it at the femtosecond timescale.

scaling suggests that the non-linear induced rotation is particularly relevant for external B-fields at THz frequencies. However, note that the linear dynamics (with the external field) would also contribute at those frequencies. Fig. 3(c) shows the second-order scaling of the magnetization dynamics with the external B-field amplitude for central frequencies of 250 THz (blue), 100 THz (red) and 50 THz (black). As expected, the total rotation increases with the B-field amplitude, being already measurable at tens of T. Finally, Fig. 3(d) depicts the total rotation of the magnetization for a B-field pulse of frequency 50 THz as a function of the pulse duration, t_p. This latter result confirms that the non-linear chiral effect presented in this work is cumulative in time, as predicted from Eq. (10).

One of the most appealing opportunities of this non-linear effect is the possibility to achieve non-thermal ultrafast all-optical switching driven solely by an external circularly polarized B-field. Based on the dependencies presented in Fig. 3, we show in Fig. 4 two different micromagnetic simulation results in which switching is achieved through the use of a RCP B-field pulse. The B-field envelopes of each case are represented in dashed-red lines, whereas the magnetization components m_x, m_y, m_z are represented in blue, yellow and black, respectively. The first case makes use of a short, 1 ps, 60 THz, 275 T B-field pulse, whereas the second case uses a 10 ps B-field pulse of 60 T and 30 THz. In both cases the m_z component reverses its direction along the course of the pulse, showing that complete switching at the fs or ps timescale can be achieved, depending on the strength, pulse duration and frequency of the B-field.

5. Discussion

Our results unveil a non-linear chiral magnetic effect driven by ultrafast circularly (or elliptically) polarized B-field pulses, lying in the plane containing the initial magnetization. This purely precessional effect is quadratic in the external B-field, and proportional to the inverse of

https://doi.org/10.1017/hpl.2023.71 Published online by Cambridge University Press

the frequency, being equivalent to a drift field that depends linearly on the gyromagnetic ratio. This non-linearity is proved to be essential at this time scale, since a linear response would follow adiabatically the magnetic field and, consequently, would restore the magnetization to its initial state after pulse is gone. Conversely, the reported drift field plays a significant role in the magnetization dynamics driven by moderately intense circularly-polarized B-fields —tens of Tesla at the ps timescale, while hundreds of Tesla at the fs timescale. Although we have studied the magnetization dynamics in CoFeB, this effect is a general feature of the LLG equation, thus being present in all ferromagnets, but also in ferrimagnets and antiferromagnets. Besides, this rectification effect may be exploited to generate THz electric currents via the inverse spin Hall effect, that would emit electromagnetic THz radiation[37] when illuminated with infrared light.

In addition, it should be stressed that, even when the E-field is non-negligible, the reported non-linear mechanism on the B-field may play a role, so a complete study of the ultrafast magnetization dynamics would require taking into account this effect. We note that recent works pointed out the need of including nutation in the dynamical equation of the magnetization[52,56,57]. This term could also lead to second-order effects. Thus, our work serves as a first step towards the investigation of higher-order phenomena induced by magnetic inertia, potentially leading to even shorter time-scale magnetization switching.

Finally, our work demonstrates that the recently developed scenario of spatially isolated fs B-fields[39,44–46] opens the path to the ultrafast manipulation of magnetization dynamics by purely precessional effects, avoiding thermal effects due to the E-field or magnetization damping. Although the spatial decoupling of the intense B-field from the E-field using fs structured pulses is technologically challenging, it is granted by the rapid development of intense ultrafast laser sources, from the infrared (800 nm, 375 THz), to the mid-infrared (4μm - 40 μm, 75 - 7 THz)[58–60]. Thinking forward, we believe that our work paves the way towards induced all-optical magnetization dynamics at even shorter timescales, towards the sub-femtosecond regime. Recent works in the generation of ultrafast structured pulses in high-order harmonic generation[61–63] may open the route towards such ultrafast control.

Acknowledgments

This work was supported by the European Research Council (ERC) under the European Union's Horizon 2020 research and innovation program (Grant Agreement No. 851201, ATTOSTRUCTURA); Ministerio de Ciencia de Innovación y Universidades (PID2020-117024GB-C41, PID2019-106910GB-I00, RYC-2017-22745); Junta de Castilla y León FEDER (SA287P18).

References

1. E. Beaurepaire, J.-C. Merle, A. Daunois, and J.-Y. Bigot. Ultrafast Spin Dynamics in Ferromagnetic Nickel. Phys. Rev. Lett., 76:4250–4253, May 1996.
2. C. D. Stanciu, F. Hansteen, A. V. Kimel, A. Kirilyuk, A. Tsukamoto, A. Itoh, and Th. Rasing. All-Optical Magnetic Recording with Circularly Polarized Light. Phys. Rev. Lett., 99:047601, Jul 2007.
3. A. B. Schmidt, M. Pickel, M. Donath, P. Buczek, A. Ernst, V. P. Zhukov, P. M. Echenique, L. M. Sandratskii, E. V. Chulkov, and M. Weinelt. Ultrafast Magnon Generation in an Fe Film on Cu(100). Phys. Rev. Lett., 105:197401, Nov 2010.
4. Phoebe Tengdin, Wenjing You, Cong Chen, Xun Shi, Dmitriy Zusin, Yingchao Zhang, Christian Gentry, Adam Blonsky, Mark Keller, Peter M. Oppeneer, Henry C. Kapteyn, Zhensheng Tao, and Margaret M. Murnane. Critical behavior within 20 fs drives the out-of-equilibrium laser-induced magnetic phase transition in nickel. Science Advances, 4(3):eaap9744, 2018.
5. N. Tesařová, P. Němec, E. Rozkotová, J. Zemen, T. Janda, D. Butkovičová, F. Trojánek, K. Olejník, V. Novák, P. Malý, and T. Jungwirth. Experimental observation of the optical spin–orbit torque. Nature Photonics, 7:492–498, 2013.
6. P. C. Lingos, J. Wang, and I. E. Perakis. Manipulating femtosecond spin-orbit torques with laser pulse sequences to control magnetic memory states and ringing. Phys. Rev. B, 91:195203, May 2015.
7. Gyung-Min Choi, André Schleife, and David G. Cahill. Optical-helicity-driven magnetization dynamics in metallic ferromagnets. Nature Communications, 8:15085, 2017.
8. A. Stupakiewicz, K. Szerenos, D. Afanasiev, , A. Kirilyuk, and A. V. Kimel. Ultrafast nonthermal photo-magnetic recording in a transparent medium. Nature, 542:71–74, February 2017.
9. C.S. Davies, T. Janssen, J.H. Mentink, A. Tsukamoto, A.V. Kimel, A.F.G. van der Meer, A. Stupakiewicz, and A. Kirilyuk. Pathways for Single-Shot All-Optical Switching of Magnetization in Ferrimagnets. Phys. Rev. Applied, 13:024064, Feb 2020.
10. G. P. Zhang and W. Hübner. Laser-Induced Ultrafast Demagnetization in Ferromagnetic Metals. Phys. Rev. Lett., 85:3025–3028, Oct 2000.
11. B. Koopmans, J. J. M. Ruigrok, F. Dalla Longa, and W. J. M. de Jonge. Unifying Ultrafast Magnetization Dynamics. Phys. Rev. Lett., 95:267207, Dec 2005.
12. Dennis Rudolf, Chan La-O-Vorakiat, Marco Battiato, Roman Adam, Justin M. Shaw, Emrah Turgut, Pablo Maldonado, Stefan Mathias, Patrik Grychtol, Hans T. Nembach, Thomas J. Silva, Martin Aeschlimann, Henry C. Kapteyn, Margaret M. Murnane, Claus M. Schneider, and Peter M. Oppeneer. Ultrafast magne-

https://doi.org/10.1017/hpl.2023.71 Published online by Cambridge University Press

tization enhancement in metallic multilayers driven by superdiffusive spin current. Nature Communications, 3:1037, 2012.

13. K. Krieger, J. K. Dewhurst, P. Elliott, S. Sharma, and E. K. U. Gross. Laser-Induced Demagnetization at Ultrashort Time Scales: Predictions of TDDFT. Journal of Chemical Theory and Computation, 11(10):4870–4874, 2015.
14. S. Bonetti, M. C. Hoffmann, M.-J. Sher, Z. Chen, S.-H. Yang, M. G. Samant, S. S. P. Parkin, and H. A. Dürr. THz-Driven Ultrafast Spin-Lattice Scattering in Amorphous Metallic Ferromagnets. Phys. Rev. Lett., 117:087205, Aug 2016.
15. Ute Bierbrauer, Sebastian T Weber, David Schummer, Moritz Barkowski, Anna-Katharina Mahro, Stefan Mathias, Hans Christian Schneider, Benjamin Stadtmüller, Martin Aeschlimann, and Baerbel Rethfeld. Ultrafast magnetization dynamics in Nickel: impact of pump photon energy. Journal of Physics: Condensed Matter, 29(24):244002, may 2017.
16. John Kay Dewhurst, Peter Elliott, Sam Shallcross, Eberhard K. U. Gross, and Sangeeta Sharma. Laser-Induced Intersite Spin Transfer. Nano Letters, 18(3):1842–1848, 2018.
17. Florian Siegrist, Julia A. Gessner, Marcus Ossiander, Christian Denker, Yi-Ping Chang, Malte C. Schröder, Alexander Guggenmos, Yang Cui, Jakob Walowski, Ulrike Martens, J. K. Dewhurst, Ulf Kleineberg, Markus Münzenberg, Sangeeta Sharma, and Martin Schultze. Light-wave dynamic control of magnetism. Nature, 571:240, 2019.
18. Phoebe Tengdin, Christian Gentry, Adam Blonsky, Dmitriy Zusin, Michael Gerrity, Lukas Hellbrück, Moritz Hofherr, Justin Shaw, Yaroslav Kvashnin, Erna K. Delczeg-Czirjak, Monika Arora, Hans Nembach, Tom J. Silva, Stefan Mathias, Martin Aeschlimann, Henry C. Kapteyn, Danny Thonig, Konstantinos Koumpouras, Olle Eriksson, and Margaret M. Murnane. Direct light-induced spin transfer between different elements in a spintronic Heusler material via femtosecond laser excitation. Science Advances, 6(3):eaaz1100, 2020.
19. M. Hofherr, S. Häuser, J. K. Dewhurst, P. Tengdin, S. Sakshath, H. T. Nembach, S. T. Weber, J. M. Shaw, T. J. Silva, H. C. Kapteyn, M. Cinchetti, B. Rethfeld, M. M. Murnane, D. Steil, B. Stadtmüller, S. Sharma, M. Aeschlimann, and S. Mathias. Ultrafast optically induced spin transfer in ferromagnetic alloys. Science Advances, 6(3):eaay8717, 2020.
20. Philippe Scheid, Sangeeta Sharma, Gregory Malinowski, Stéphane Mangin, and Sébastien Lebègue. Ab Initio Study of Helicity-Dependent Light-Induced Demagnetization: From the Optical Regime to the Extreme Ultraviolet Regime. Nano Letters, 21(5):1943–1947, 2021.
21. A. L. Chekhov, Y. Behovits, J. J. F. Heitz, C. Denker, D. A. Reiss, M. Wolf, M. Weinelt, P. W. Brouwer, M. Münzenberg, and T. Kampfrath. Ultrafast Demagnetization of Iron Induced by Optical versus Terahertz Pulses. Phys. Rev. X, 11:041055, Dec 2021.
22. A. V. Kimel, A. Kirilyuk, P. A. Usachev, R. V. Pisarev, A. M. Balbashov, and Th. Rasing. Ultrafast non-thermal control of magnetization by instantaneous photomagnetic pulses. Nature, 435:655–657, 2005.
23. Hanan Hamamera, Filipe Souza Mendes Guimarães, Manuel dos Santos Dias, and Samir Lounis. Polarisation-dependent single-pulse ultrafast optical switching of an elementary ferromagnet. Communications Physics, 5:16, 2022.
24. J. Wätzel, Y. Pavlyukh, A. Schäffer, and J. Berakdar. Optical vortex driven charge current loop and optomagnetism in fullerenes. Carbon, 99:439–443, 2016.
25. G. P. Zhang, Y. H. Bai, and Thomas F. George. Switching ferromagnetic spins by an ultrafast laser pulse: Emergence of giant optical spin-orbit torque. EPL (Europhysics Letters), 115(5):57003, sep 2016.
26. A. Stupakiewicz, C. S. Davies, K. Szerenos, D. Afanasiev, K. S. Rabinovich, A. V. Boris, A. Caviglia, A. V. Kimel, and A. Kirilyuk. Ultrafast phononic switching of magnetization. Nature Physics, 17:489–492, 2021.
27. I. Tudosa, C. Stamm, A. B. Kashuba, F. King, H. C. Siegmann, J. Stöhr, G. Ju, B. Lu, and D. Weller. The ultimate speed of magnetic switching in granular recording media. Nature, 428:831–833, 2004.
28. S. Wienholdt, D. Hinzke, and U. Nowak. THz Switching of Antiferromagnets and Ferrimagnets. Phys. Rev. Lett., 108:247207, Jun 2012.
29. C. Vicario, C. Ruchert, F. Ardana-Lamas, P. M. Derlet, B. Tudu, J. Luning, and C. P. Hauri. Off-resonant magnetization dynamics phase-locked to an intense phase-stable terahertz transient. Nature Photonics, 7:720–723, 2013.
30. Lars Bocklage. Model of THz Magnetization Dynamics. Scientific Reports, 6:22767, 2016.
31. T. G. H. Blank, K. A. Grishunin, E. A. Mashkovich, M. V. Logunov, A. K. Zvezdin, and A. V. Kimel. THz-Scale Field-Induced Spin Dynamics in Ferrimagnetic Iron Garnets. Phys. Rev. Lett., 127:037203, Jul 2021.
32. B. C. Choi, K. Jordan, J. Rudge, and Th. Speliotis. Coherent Magnetization Dynamics in Ni80Fe20 Thin Films Incorporated in Fe/Au Spintronic Terahertz Emitters. IEEE Transactions on Magnetics, 57(2):1–4, 2021.
33. Xingyu Yang, Ye Mou, Bruno Gallas, Agnès Maitre, Laurent Coolen, and Mathieu Mivelle. Tesla-range femtosecond pulses of stationary magnetic field, optically generated at the nanoscale in a plasmonic

https://doi.org/10.1017/hpl.2023.71 Published online by Cambridge University Press

antenna. ACS Nano, 16(1):386–393, 2022.

34. Mostafa Shalaby, Andreas Donges, Karel Carva, Rolf Allenspach, Peter M. Oppeneer, Ulrich Nowak, and Christoph P. Hauri. Coherent and incoherent ultrafast magnetization dynamics in $3d$ ferromagnets driven by extreme terahertz fields. Phys. Rev. B, 98:014405, Jul 2018.
35. T. Kampfrath, M. Battiato, P. Maldonado, G. Eilers, J. Nötzold, S. Mährlein, V. Zbarsky, F. Freimuth, Y. Mokrousov, S. Blügel, M. Wolf, I. Radu, P. M. Oppeneer, and M. Münzenberg. Terahertz spin current pulses controlled by magnetic heterostructures. Nature Nanotechnology, 8:256–260, 2013.
36. Peter Salén, Martina Basini, Stefano Bonetti, János Hebling, Mikhail Krasilnikov, Alexey Y. Nikitin, Georgii Shamuilov, Zoltán Tibai, Vitali Zhaunerchyk, and Vitaliy Goryashko. Matter manipulation with extreme terahertz light: Progress in the enabling THz technology. Physics Reports, 836-837:1–74, 2019.
37. Tom S. Seifert, Liang Cheng, Zhengxing Wei, Tobias Kampfrath, and Jingbo Qi. Spintronic sources of ultrashort terahertz electromagnetic pulses. Applied Physics Letters, 120(18):180401, 2022.
38. Qiwen Zhan. Cylindrical vector beams: from mathematical concepts to applications. Advances in Optics and Photonics, 1(1):1, January 2009.
39. Manuel Blanco, Ferran Cambronero, M. Teresa Flores-Arias, Enrique Conejero Jarque, Luis Plaja, and Carlos Hernández-García. Ultraintense Femtosecond Magnetic Nanoprobes Induced by Azimuthally Polarized Laser Beams. ACS Photonics, 6(1):38–42, 2019.
40. Caner Guclu, Mehdi Veysi, and Filippo Capolino. Photoinduced Magnetic Nanoprobe Excited by an Azimuthally Polarized Vector Beam. ACS Photonics, 3(11):2049–2058, 2016.
41. Jinwei Zeng, Fei Huang, Caner Guclu, Mehdi Veysi, Mohammad Albooyeh, H. Kumar Wickramasinghe, and Filippo Capolino. Sharply Focused Azimuthally Polarized Beams with Magnetic Dominance: Near-Field Characterization at Nanoscale by Photoinduced Force Microscopy. ACS Photonics, 5(2):390–397, 2018.
42. Jinwei Zeng, Mahsa Darvishzadeh-Varcheie, Mohammad Albooyeh, Mohsen Rajaei, Mohammad Kamandi, Mehdi Veysi, Eric O. Potma, Filippo Capolino, and H. K. Wickramasinghe. Exclusive Magnetic Excitation Enabled by Structured Light Illumination in a Nanoscale Mie Resonator. ACS Nano, 12(12):12159–12168, 2018.
43. Jiaan Cao, Lyuzhou Ye, Dawei He, Xiao Zheng, and Shaul Mukamel. Magnet-Free Time-Resolved Magnetic Circular Dichroism with Pulsed Vector Beams. The Journal of Physical Chemistry Letters, 13(48):11300–11306, 2022.
44. Shawn Sederberg, Fanqi Kong, Felix Hufnagel, Chunmei Zhang, Ebrahim Karimi, and Paul B Corkum. Vectorized optoelectronic control and metrology in a semiconductor. Nature Photonics, 14(11):680–685, 2020.
45. Shawn Sederberg, Fanqi Kong, and Paul B. Corkum. Tesla-Scale Terahertz Magnetic Impulses. Phys. Rev. X, 10:011063, Mar 2020.
46. K Jana, K R Herperger, F Kong, Y Mi, C Zhang, P B Corkum, and S Sederberg. Reconfigurable electronic circuits for magnetic fields controlled by structured light. Nature Photonics, 15(8):622–626, 2021.
47. Yin Shi, David R Blackman, and Alexey Arefiev. Electron acceleration using twisted laser wavefronts. Plasma Physics and Controlled Fusion, 63(12):125032, nov 2021.
48. Matthias Hudl, Massimiliano d'Aquino, Matteo Pancaldi, See-Hun Yang, Mahesh G. Samant, Stuart S. P. Parkin, Hermann A. Dürr, Claudio Serpico, Matthias C. Hoffmann, and Stefano Bonetti. Nonlinear Magnetization Dynamics Driven by Strong Terahertz Fields. Phys. Rev. Lett., 123:197204, Nov 2019.
49. R. A. Fonseca, L. O. Silva, F. S. Tsung, V. K. Decyk, W. Lu, C. Ren, W. B. Mori, S. Deng, S. Lee, T. Katsouleas, and J. C. Adam. OSIRIS: A Three-Dimensional, Fully Relativistic Particle in Cell Code for Modeling Plasma Based Accelerators. In Peter M. A. Sloot, Alfons G. Hoekstra, C. J. Kenneth Tan, and Jack J. Dongarra, editors, Computational Science — ICCS 2002, pages 342–351, Berlin, Heidelberg, 2002. Springer Berlin Heidelberg.
50. R A Fonseca, S F Martins, L O Silva, J W Tonge, F S Tsung, and W B Mori. One-to-one direct modeling of experiments and astrophysical scenarios: pushing the envelope on kinetic plasma simulations. Plasma Physics and Controlled Fusion, 50(12):124034, 2008.
51. R A Fonseca, J Vieira, F Fiuza, A Davidson, F S Tsung, W B Mori, and L O Silva. Exploiting multi-scale parallelism for large scale numerical modelling of laser wakefield accelerators. Plasma Physics and Controlled Fusion, 55(12):124011, 2013.
52. J.-E. Wegrowe and M.-C. Ciornei. Magnetization dynamics, gyromagnetic relation, and inertial effects. American Journal of Physics, 80(7):607–611, 2012.
53. A. Vansteenkiste, J. Leliaert, M. Dvornik, M. Helsen, F. Garcia-Sanchez, and B. Van Waeyenberge. The design and verification of MuMax3. AIP Advances, 4:107133, 2014.
54. G. Bertotti, I. D. Mayergoyz, and C. Serpico. Analysis of instabilities in nonlinear Landau–Lifshitz–Gilbert dynamics under circularly polarized fields. Journal of Applied Physics, 91(10):7556–7558, 2002.
55. Massimiliano d'Aquino, Claudio Serpico, Giorgio Bertotti, Isaak D. Mayergoyz, and Roberto Bonin. Nonlinear Resonant and Chaotic Dynamics in Microwave Assisted Magnetization Switching. IEEE Transactions

https://doi.org/10.1017/hpl.2023.71 Published online by Cambridge University Press

on Magnetics, 45(10):3950–3953, 2009.

56. M.-C. Ciornei, J. M. Rubí, and J.-E. Wegrowe. Magnetization dynamics in the inertial regime: Nutation predicted at short time scales. Phys. Rev. B, 83:020410, Jan 2011.
57. Kumar Neeraj, Nilesh Awari, Sergey Kovalev, Debanjan Polley, Nanna Zhou Hagström, Sri Sai Phani Kanth Arekapudi, Anna Semisalova, Kilian Lenz, Bertram Green, Jan-Christoph Deinert, Igor Ilyakov, Min Chen, Mohammed Bawatna, Valentino Scalera, Massimiliano d'Aquino, Claudio Serpico, Olav Hellwig, Jean-Eric Wegrowe, Michael Gensch, and Stefano Bonetti. Inertial spin dynamics in ferromagnets. Nature Physics, 17:245–250, 2021.
58. V Shumakova, P Malevich, S Ališauskas, A Voronin, A M Zheltikov, D Faccio, D Kartashov, A. Baltuška, and A Pugzlys. Multi-millijoule few-cycle mid-infrared pulses through nonlinear self-compression in bulk. Nature Communications, 7(1):12877, 2016.
59. Claudia Gollner, Mostafa Shalaby, Corinne Brodeur, Ignas Astrauskas, Rokas Jutas, Evan Constable, Lorenz Bergen, Andrius Baltuška, and Audrius Pugžlys. Highly efficient THz generation by optical rectification of mid-IR pulses in DAST. APL Photonics, 6(4):046105, 2021.
60. Ugaitz Elu, Luke Maidment, Lénárd Vámos, Francesco Tani, David Novoa, Michael H Frosz, Valeriy Badikov, Dmitrii Badikov, Valentin Petrov, Philip St J Russell, and Jens Biegert. Seven-octave high-brightness and carrier-envelope-phase-stable light source. Nature Photonics, 15(4):277–280, 2021.
61. Carlos Hernández-García, Alex Turpin, Julio San Román, Antonio Picón, Rokas Drevinskas, Ausra Cerkauskaite, Peter G. Kazansky, Charles G. Durfee, and Í nigo J. Sola. Extreme ultraviolet vector beams driven by infrared lasers. Optica, 4(5):520–526, May 2017.
62. Carlos Hernández-García, Laura Rego, Julio San Román, Antonio Picón, and Luis Plaja. Attosecond twisted beams from high-order harmonic generation driven by optical vortices. High Power Laser Science and Engineering, 5:e3, 2017.
63. Alba de las Heras, Alok Kumar Pandey, Julio San Román, Javier Serrano, Elsa Baynard, Guillaume Dovillaire, Moana Pittman, Charles G. Durfee, Luis Plaja, Sophie Kazamias, Olivier Guilbaud, and Carlos Hernández-García. Extreme-ultraviolet vector-vortex beams from high harmonic generation. Optica, 9(1):71–79, 2022.

https://doi.org/10.1017/hpl.2023.71 Published online by Cambridge University Press